Advances in Materials Science Research

Maryann C. Wythers
Editor

NOVA

ADVANCES IN MATERIALS SCIENCE RESEARCH.

VOLUME 1

MARYANN C. WYTHERS
EDITOR

Nova Science Publishers, Inc.
New York

LIBRARY OF CONGRESS CATALOGING-IN-PUBLICATION DATA

ISSN: 2159-1997

ISBN: 978-1-61728-109-9

Published by Nova Science Publishers, Inc. † New York

ADVANCES IN MATERIALS SCIENCE RESEARCH.

VOLUME 1

ADVANCES IN MATERIALS SCIENCE RESEARCH

Additional books in this series can be found on Nova's website under the Series tab.

Additional E-books in this series can be found on Nova's website under the E-book tab.

PREFACE

Materials science includes those parts of chemistry and physics that deal with the properties of materials. It encompasses four classes of materials, the study of each which may be considered a separate field: metals, ceramics, polymers and composites. Materials science is often referred to as materials science and engineering because it has many applications. This new volume gathers important research from around the globe in this dynamic field including the detection and toughening of microcracks, electrospinning materials and applications, cement, concrete and composite processing, and applications and paramagnetism.

Chapter 1 summarizes the results of research work done by the present author and his colleagues on the micromechanism of cleavage fracture in precracked specimens made of HSLA steel and weld metal at low temperatures. Three parts are involved:

1. Three Sequential Non-Stop Stages Comprise the Cleavage Fracture Process: A typical cleavage fracture process is composed of the following three sequential stages:(1) Crack nucleation by breaking second phase particle, (2) Second phase particle-crack propagation across the barrier of particle/matrix boundary, (3) Ferrite grain-crack propagation across the barrier of matrix grain/matrix grain.

2. Mechanism and Types of Crack Nucleation: Five mechanisms of crack nucleation are observed in our work: (1) plastic slip-induced particle-cracking; (2) shear stress-induced fiber-loading cracking; (3) decohesion of inclusion boundary; (4) blocky hard-particle-induced delamination; (5) plastic strain-induced ferrite cracking.

Six types of crack nucleation origins are observed in our work: (1)carbide particle, (2)M-A constituent, (Martensite-Austenite constituent), (3) non-metallic inclusion, (4) pearlite in ferrite steel, (5) carbide/ferrite aggregates formed by decomposed M-A island, (6) crack nucleated in ferrite or bainite matrix.

3. Mechanism of Cleavage Microcrack Growth: The results reveal that the micro-mechanisms of cleavage cracking are variable with the variation of temperatures. In the lower shelf transition temperature region, three sub-regions are distinguished where the mechanisms of cleavage cracking appear in different modes: (1)at the lower end temperatures (the first sub-region, <-130°C) the cleavage is controlled by crack nucleation at the microscopic scale and is driven by an increasing applied load that blunts the precrack tip at the macroscopic scale, (2) at moderate low temperatures (the second sub-region, -130°C to -90°C) the cleavage fracture is controlled by the propagation of a carbide-sized crack into contiguous grain at the microscopic scale and is also driven by the increasing applied load that further blunts the

precrack tip at the macroscopic scale, (3) at the upper end temperature (the third sub-region, -80°C to -60°C), for compensating the drop of the yield stress in addition to the precrack tip blunting a short fibrous crack is needed to extend from the precrack tip to increase the peak normal stress and to move it closer to the precrack tip.

In the transition temperature region, the critical event for cleavage fracture shifts from the propagation of a carbide-sized crack into matrix grain to the propagation of a grain-sized crack into contiguous grains. The cleavage cracking is controlled by the propagation of a grain-sized crack into contiguous grains. It is always preceded by a fibrous crack, which increases the stress triaxiality and the peak normal stress and to move the peak normal stress closer to the precrack tip. The minimum length of the fibrous crack has a definite relationship with the temperature and determines the lower-envelop line of the toughness transition curve.

Creep damage in steels is a topic of great complexity and enormous engineering importance, especially in energy production industry. The long-lasting exposure to high temperatures and stresses leads to the formation of microcracks in the material by the end of the secondary creep, which - if not timely detected - may coalesce and eventually bring the component to costly and dangerous brittle failures. At the microscale, the actual damage process depends on the type of steel. Chapter 2 offers a critical overview of creep in steels, with emphasis on power plant components, through an excursus organized in four major parts, namely: (i) a brief review of creep (macro and micro) mechanisms, (ii) technical standards, (iii) creep management by damage detection in low alloy steel via field metallography and non destructive replication technique, and (iv) new modeling routes to simulate quasi-brittle failure processes via statistical damage mechanics. In spite of the broad scope, this chapter does not aim at a comprehensive treatment of the subject, but rather provides an "integrated" perspective of it, parading the many viewpoints purported by different operators (i.e. material scientists, physicists, designers, field engineers, technicians, legislators, etc.). The chapter stems from ISPESL extensive tradition in issuing standards and guidelines for creep design and inspection of steel components at the national and EU level.

In Chapter 3 the authors summarize the results of research work obtained in recent years on the mechanisms of cracking, fracturing and toughening of TiAl alloys.

1. Mechanism of Microcrack Initiation and Propagation: Microcracks prefer to be initiated and propagated along lamellar interfaces. In a thin tensile specimen, cracks are initiated within an elastic environment without preceding plastic strain. The driving force for initiating a cleavage crack is the tensile stress rather than the shear stress. If in front of the growing microcrack there is a barrier grain with a lamellar orientation unfavorable for the crack propagation, the propagation of crack can take three ways: (1) a new crack is initiated along the lamellar interface in a grain ahead of the barrier grain, then the barrier grain is cracked by translamellar cleavage; (2) bypasses the barrier grain by skipping through the grain boundary or along the inclined interface inside the grain(deflection or bifurcation of crack); (3) directly crosses the barrier grain by translamellar cracking.

2. Global Fracture Mechanism of Specimen: Global fracture of TiAl specimens is induced by microcrack propagation in two ways, one is the Critical crack triggering-fracture, that is: when a microcrack extends to a critical length which acts as a Griffiths crack and matches the loading stress the crack propagates catastrophically through the entire specimen., the other is accumulated damage-induced fracture, that is: when a great number of large interlamellar cracks are produced prior to final fracture, which decrease the area of the cross section and seriously weaken the material. The final fracture happens by connection of

interlamellar cracks on a most damaged section, where the highest density of microcracks is accumulated.

3. Mechanism of Reverse Dependences of Tensile Strength and Notch Toughness on the Grain Sizes: The phenomena of reverse dependences of tensile strength and notch toughness on the grain sizes are explained with the above fracture models.

4. Effect of Damage: Two types of effects of cracking-damage are revealed: When a displacement-controlled tensile test is performed at a lower strain speed the effects of microcrack-damage can be summarized as: The volumetric effects which weaken the material by reducing the elastic modulus and produce a stress-softening sector in load-displacement curve and the facial effects which decrease the area of the cross section and the final fracture stress of specimen.

5. Toughening Mechanisms: The main toughening mechanisms in FL specimens are illustrated as: deflection and bifurcation of the main crack, blunting of the crack tip and formation of a diffuse zone of microcracks. The cracking-bridging effects are sub-effective.

6. Fatigue Fracture Mechanism and Compression Fracture Mechanism: Fatigue fracture mechanism and compression deformation and fracture behavior are also discussed in detail.

Large-scale concrete structures, such as long-span bridges, hydraulic dams, and high-rise buildings, have increasingly been exposed to multi-hazard environments in recent years. Understanding the behavior of concrete under earthquake and blast loads becomes more urgent and important in the design of these engineering structures. Chapter 4 briefly introduces the research significance and measurement for the dynamic properties of concrete at high strain rates. The mechanical parameters of concrete under uniaxial dynamic loading conditions were obtained and compared with the static properties that have been widely used in design codes. A special test apparatus and procedure was designed and presented in order to evaluate the main concrete characteristics under multiaxial dynamic loading and to understand various failure mechanisms in one-, two-, and three-dimensional loading conditions. The failure modes of concrete were investigated. Based on a comprehensive test program, material specifications are recommended for the seismic design of concrete structures.

Rare earth oxide thin films are of interest for several purposes including optical coatings, catalytic agents and/or supports, protective coatings, *etc.* Among the rare earth oxides, praseodymium oxides have been studied for many applications, such as component of varistor ceramic materials, photocatalytically active materials, anode for organic light-emitting diodes and as dielectrics for microelectronics applications. The most studied praseodymium dielectrics include: *h*-Pr_2O_3, praseodymium silicates and praseodymium aluminates. In Chapter 5, a description of the different MOCVD approaches to fabricate praseodymium oxides, silicates and aluminates thin films with dielectric properties is presented. Thus, in the following, the MOCVD approach to grow pure Pr-containing materials is discussed ranging from the precursors to the deposition parameters. Moreover, a detailed characterization of the final structure of the deposited films is supplied since it is mandatory in order to achieve a fundamental understanding of the electronic properties in the perspective of their applications in microelectronics devices.

Measurement of stiffness and ultimate strength of biological tissues is a relatively common task in experimental biomechanics. Most of the papers published on microcracks of biological tissues deal with calcified tissue, especially with bone. Surprisingly, quantitative microscopic assessment of microcracks produced by the experiments in soft tissues is rarely

performed and published. Evaluation of spatial relationship between microcracks and main histological constituents of organ samples can prove which of the tissue constituents offer more or less resistance during biomechanical experiments. First part of Chapter 6 gives a review on quantitative microscopical assessment of porosities in the compact bone. The bone is perforated by a network of osteocyte lacunes and vascular canals. Some papers suggest that there is a relation between the osteocyte lacunar-canalicular network, vascular canals, and microdamage accumulation in the bone matrix. Three useful stereological methods are presented: the optical disector for assessing locally specific numerical density of osteocyte lacunes, the point-counting method for estimating area fraction of vascular canals, and the Delaunay triangulation for analysis of anisotropy of the vascular canals. As producing microcracks goes hand in hand with measurement of mechanical parameters in these biological samples, the identification of the Young's moduli and ultimate strength is included in this review. Therefore the second part of the paper deals with methods and routines used for evaluation of mechanical parameters in biological tissues. The third part of this contribution is focused on a simple method useful to determine which constituent of any soft tissue offers less resistance during biomechanical experiments, such as drop shatter tests or ultimate strength tests. This two-dimensional approach is based on histological sections and estimation of the intensity of intersections between microcracks and tissue constituents under study (e.g., fibres, tubules, etc.) with a known length density. The solution is to apply a simple stereological method to discriminate between random and tissue-specific propagation of microcracks.

Damage and fracture in composite materials are complicated evolutionary phenomena. Due to difficulty in better understanding of the complicated phenomena, crucial researches on the evolution of damage up to fracture are still carried out to predict the overall behavior of composite materials. Among a variety of damage factors, the microcrack propagation, from nucleation to growth, significantly affect the macroscopic behavior of composite materials such as nonlinear behavior, degradation of mechanical properties, significant volume dilation, etc. A variety of damage mechanics based models, which provide an effective framework for the description of damage including nucleation, growth, and coalescence of microcracks, have been developed to predict the damage and failure processes in composite materials. In these damage mechanics based models, there are two main classes of damage models, i.e., macromechanical and micromechanical approaches. The microscale damage based models, which treat each microphase as a statistically homogeneous medium, are reviewed in Chapter 7. Specially, the damage propagation on nucleation and growth of microcrack in brittle composite materials is mainly discussed in the chapter.

Paramagnetic endohedral fullerenes ($A@C_{2n}$) are compounds that contain a paramagnetic atom (A) inside the fullerene cage C_{2n}. The purpose of Chapter 8 is to highlight examples of progress in chemical physics of these compounds and point out fertile grounds for future applications of $A@C_{2n}$ in nanoengineering and medicine. The atoms entrapped inside the cage often manifest unusual properties. In paramagnetic endometallofullerenes ($M@C_{2n}$) there is the partial runoff of electron spin density outside the fullerene cage ("spin leakage") testified by EPR, ENDOR and NMR data. In paramagnetic $N@C_{60}$, $P@C_{60}$, on the other hand, there is the accumulation of electron spin density on the entrapped atoms as if the electronic shells of the entrapped atoms are compressed ("spin compression"). The magnetic resonance imaging (MRI) seems to be fruitful field for application of paramagnetic M@C2n in medicine. For example, the water proton relaxivity of some $Gd@C_{82}(OH)_n$ is much higher

than that of Gd(III)-DTPA which is now in clinical use as the contrast agent for magnetic resonance imaging. In nanotechnology, paramagnetic endohedral fullerenes hold much promise as the basic elements for realizing nanometer scale devices, amongst them – molecular magnets, superconductors with low critical temperatures, molecular memory devices, field effect transistors, quantum dots, fullerene-based quantum computers.

Food science research has increasingly focused on using polymer nanofibers in areas such as active packaging and additive encapsulation. The high surface-to-volume ratio due to the small nanofiber sizes favors the increased nanoeffects, which include increased surface reactivity, high strength to weight ratio, and higher thermal conductivity. The electrospinning process yields these nanofibers through a simple and flexible method. The basic electrospinning setup includes a polymer solution in a syringe, conductive collector, and voltage source with wires attached to the syringe and collector. The electrospinning parameters (i.e. applied electric field, solution flow rate, and distance from syringe tip to collector) are tuned in order to modify fiber properties such as morphology, porosity and sizes to tailor the fiber mats according to the desired function and application. Chapter 9 reviews previous studies on electrospun synthetic polymers for food applications and highlights the recent studies and advances in using biopolymer nanofibers, which are renewable, biocompatible and biodegradable materials, for applications in the development of active food packaging solutions, food coatings, additive encapsulation, flavor enhancement and delivery and nutraceutical applications.

Chapter 10 presents a study on the effects of rice-husk ash (RHA) as supplementary cementing material. The behavior of cementititious products varies with the source of the RHA. Two different RHAs, both amorphous and partially cristalline, and different replacement percentages of cement by RHA, are reported. The optimization of the RHA partially cristalline for their use as supplementary cementing material is presented. The properties investigated included setting times, autogenous deformation, compressive strength, splitting tensile strength, modulus of rupture, modulus of elasticity, air permeability, chloride penetration ions, alkali-silica expansion, acid and sulfate resistance. The results were compared with those of the reference without RHA. From the tested properties, it is concluded that the two types of ash used provide a possitive effect and reveal the holistic behavior of the RHA as supplementary cementing material.

Diluted magnetic semiconductor (DMS) generically encompasses a wide range of semiconductor alloys formed by the substitutional introduction of magnetic ions into a compound semiconductor. Taken in this most general sense, DMS materials include such diverse systems as $Zn_{1-x}Mn_xSe$, $Pb_{1-x}Eu_xTe$ and $(Cd_{1-x}Mn_x)_2As_3$. In $A_{1-x}{}^{II}Mn_xB^{VI}$ ternary alloy, Mn^{++} is randomly substituted for the cation of a II-VI semiconductor. It has gained much attention recently. The presence of the manganese ions Mn^{++} in $A_{1-x}{}^{II}MnxB^{VI}$ leads to an exchange interaction between the *sp* band electrons and the *d* electrons associated with Mn^{++} in the magnetic field, resulting in a series of dramatic new effects, such as the giant Faraday rotation, the magnetic-field-induced metal-insulator transition, the occurrence of large positive *g* factor, vanishing of Shubnikov-de Haas oscillations and giant negative magnetoresistance.

In Chapter 11, the magnetic susceptibility and magnetization of $Hg_{0.89}Mn_{0.11}Te$ under a series of constant temperature and magnetic field strength will be studied. The dependence of resistivity of $Hg_{0.89}Mn_{0.11}Te$ on the magnetic field up to 6.5 Tesla, and the temperature from 5

K to 200 K are also presented. Finally, the room-temperature Faraday rotation of $Cd_{1-x}Mn_xTe$ (x=0.1, 0.2) were measured.

In Chapter 12 the electrochemical technique is applied to accelerate chloride ion migration in cement-based material to estimate its migration coefficient. The chloride migration coefficient of cement-based material was obtained by using the accelerated chloride migration test (ACMT) and measured as a function of volume fraction of aggregate and the total lateral surface area of aggregate. In order to investigate the chloride migration coefficient of percolated ITZ on the chloride migration coefficient of specimen, specimens with cylindrical aggregates of the same height as the specimen were cast and tested. The volume fraction of aggregate is constant, and the varied lateral surface area of the aggregate cylinder was obtained by using different diameters and number of aggregate. A model obtained for the migration coefficient of cement-based material, and the regression analysis is used to determine the approximate chloride migration coefficient of the percolated ITZ. Based on the experimental and regression analytical results, the approximate percolated ITZ migration coefficient is approximate 40 to 35 times of the altered migration coefficient of matrix mortar for the w/c ratio of 0.35 to 0.55.

As discussed in Chapter 13, damage present in a material in the form of plane cracks induces the decrease of some of its mechanical properties. For example, in the case of a tensile loading, and according to the plane in which the cracks are located, a decrease of the axial modulus can be observed. The same observation can be made for the shear modulus in the case of a shear loading. If the sign of the loading changes, the axial modulus is restored. It is not the case for the shear modulus. This effect is usually called the unilateral effect of damage or damage activation/deactivation.

Chapter 14 deals with damage-induced anisotropy and the indetermination of damage tensor at rest.

CONTENTS

In: Advances in Materials Science Research.Volume 1
Editor: Maryann C. Wythers, pp. 1-56
ISBN: 978-1-61728-109-9

Chapter 1

NUCLEATION AND GROWTH OF CLEAVAGE MICROCRACK IN HSLA STEEL - MICROMECHANISM FOR CLEAVAGE FRACTURE

J.H. Chen*

State Key Laboratory of Advanced Non-ferrous Metal Materials,
Lanzhou University of Technology, Lanzhou 730050, China

Abstract

This chapter summarizes the results of research work done by the present author and his colleagues on the micromechanism of cleavage fracture in precracked specimens made of HSLA steel and weld metal at low temperatures. Three parts are involved:

1. Three Sequential Non-Stop Stages Comprise the Cleavage Fracture Process

A typical cleavage fracture process is composed of the following three sequential stages:(1) Crack nucleation by breaking second phase particle, (2) Second phase particle-crack propagation across the barrier of particle/matrix boundary, (3) Ferrite grain-crack propagation across the barrier of matrix grain/matrix grain.

2. Mechanism and Types of Crack Nucleation

Five mechanisms of crack nucleation are observed in our work: (1) plastic slip-induced particle-cracking; (2) shear stress-induced fiber-loading cracking; (3) decohesion of inclusion boundary; (4) blocky hard-particle-induced delamination; (5) plastic strain-induced ferrite cracking.
Six types of crack nucleation origins are observed in our work: (1)carbide particle, (2)M-A constituent, (Martensite-Austenite constituent), (3) non-metallic inclusion, (4) pearlite in ferrite steel, (5) carbide/ferrite aggregates formed by decomposed M-A island, (6) crack nucleated in ferrite or bainite matrix.

3. Mechanism of Cleavage Microcrack Growth

The results reveal that the micromechanisms of cleavage cracking are variable with the variation of temperatures. In the lower shelf transition temperature region, three sub-regions are distinguished where the mechanisms of cleavage cracking appear in different modes:

* E-mail address: zchen@lut.cn. (Corresponding author)

(1) at the lower end temperatures (the first sub-region, <-130°C) the cleavage is controlled by crack nucleation at the microscopic scale and is driven by an increasing applied load that blunts the precrack tip at the macroscopic scale,
(2) at moderate low temperatures (the second sub-region, -130°C to -90°C) the cleavage fracture is controlled by the propagation of a carbide-sized crack into contiguous grain at the microscopic scale and is also driven by the increasing applied load that further blunts the precrack tip at the macroscopic scale,
(3) at the upper end temperature (the third sub-region, -80°C to -60°C), for compensating the drop of the yield stress in addition to the precrack tip blunting a short fibrous crack is needed to extend from the precrack tip to increase the peak normal stress and to move it closer to the precrack tip.

In the transition temperature region, the critical event for cleavage fracture shifts from the propagation of a carbide-sized crack into matrix grain to the propagation of a grain-sized crack into contiguous grains. The cleavage cracking is controlled by the propagation of a grain-sized crack into contiguous grains. It is always preceded by a fibrous crack, which increases the stress triaxiality and the peak normal stress and to move the peak normal stress closer to the precrack tip. The minimum length of the fibrous crack has a definite relationship with the temperature and determines the lower-envelop line of the toughness transition curve.

1. Introduction

This chapter summarizes the results of research work done by the present author and his colleagues on the micromechanism of cleavage fracture in precracked specimens made of HSLA steel and weld metal at low temperatures. This chapter puts forward a comprehensive framework of the cleavage fracture micromechanism for HSLA steel. This model describes the processes, driving force, critical events and criteria for cleavage crack nucleation and growth. The statements intend to amend the following concepts in the cleavage fracture mechanism which are popularly accepted and applied.

(1) Neglecting cleavage fracture being an integrative process composed of three sequential and non-stop stages (i.e. crack nucleation in a second phase particle, crack propagation through the particle-grain boundary, crack propagation through the grain-grain boundary). A rather simple model is popularly adopted, which assumes that all possible critical particle-cracks are nucleated at the onset of plastic deformation and with the normal stress increasing to a critical value, one eligible particle-crack propagates unstably. In this simple model the critical step for nucleating a microcrack is overlooked.
(2) Unique physical model (RKR model), unique critical event (particle-sized crack propagation through the particle-grain boundary), unique critical length (particle size) and unique criterion (stress criterion $\sigma_{yy} \geq \sigma_f$) are adopted for various conditions of temperatures, specimen configurations, loading rates, loading histories and microstructures.
(3) Because of setting the just yielding as the condition for Smith's formula, the normal stress induced by the dislocation pile-up is underestimated. Thereby the effects of the plastic strain-work hardening on raising the normal stress to trigger the cleavage fracture are ignored. Recent study found that in the cleavage cracking process the

plastic strain contributed not only to the crack nucleation but also to the crack propagation through work hardening.

(4) The concept of the weakest link is applied to almost all the cases. It tacitly confirms that the thermodynamic conditions (the necessary conditions) which define the sufficient accumulation of elastic energy for crack propagation throughout the whole specimen, have been satisfied. In this case the kinetic conditions (the sufficient conditions) which define the sufficient stress, strain to trigger the fracture, are the only critical criteria to be reached. However in some cases (extra-high yield stress, acute defect tip, low local fracture stress, and heterogeneous microstructure) the accumulation of the elastic energy is insufficient to propagate the nucleated crack throughout the whole specimen. In this case the concept of the weakest link is invalid and not suitable to use for a statistical model.

(5) Confusing the physical definition with the statistical results. Many critical parameters (such as the minimum distance for a cleavage site, the minimum fracture toughness, the lower-envelope line of the toughness transition curve) have definite physical meanings and the measured values scatter from these minimum values upward. In some statistical models the minimum values of these parameters are taken as statistical values which are set at a certain probability value such as 5%. These models think the measured values being scattered from a middle value both upward and downward.

The following physical model (micromechanism) summarizes the research results of the author and his colleagues. It will give a comprehensive explanation on the above issues.

2. A General Description of the Comprehensive Framework for the Micromechanism of Cleavage Fracture

Based on the results of research work on the physical model of cleavage fracture, which the present author and his colleagues have devoted themselves to for more than two and a half decades, a new framework for the micromechanism of cleavage fracture of steel is presented. It is described in the following sections. First a general Figure is depicted in this section. Then three critical steps comprising the cleavage fracture are described in detail in the following separated sections.

The materials used in the experiments were C-Mn steel, low carbon multi-minor-allying HSLA steel, 8% Ni high strength steel and weld metal. Their compositions are listed in Table 1.

Table 1. Compositions of used steels (wt%)

Steel C		Mn	Si	Ni	Mo	Cr	V	Ti	B	O	N
C-Mn	0.18	1.40	0.36								
HSLA	0.054	1.36	0.23		0.21	0.19	0.03		0.0017		
8% Ni	0.03	0.79		8	0.61	0.62					
C-Mn weld	0.07	1.24	0.28					0.03		0.03	0.019
Ti-B weld	0.05	1.45	0.48					0.03	0.004	0.03	0.019

The types of specimens used for fracture toughness measurement were: four point bending(4PB) notched specimen of Griffith-Owen size(Griffith and Owen,1971), double notched 4PB specimen, three point bending precracked specimen(standard COD specimen).

Most tests were carried out under static loading condition using the universal test machine. The instrumented Charpy V tester was used for impact tests. Test temperature ranged from -196℃ to room temperature. Temperatures were controlled by spraying liquid nitrogen into the test chamber. In-situ tensile tests were performed in vacuum using a calibrated loading stage set in a SEM. Records of the extended crack configurations are made by the SEM simultaneously with increase in the applied load.

Microstructures and the fracture surfaces were observed by OP, TEM and SEM. The phase structures were identified by selected area electron deflection in the TEM. EDX and EPMA were used by SEM and Electron probe (EPMA-1600) to analyze the compositions of second phase particles and identify their types.

Commercial FEM code ABQUES was used to calculate the stress and strain distributions ahead of a defect tip and simulate the extension of the fibrous crack.

Refer to relative papers by Chen for the detailed experimental.

The general picture of the new framework for the micromechanism of cleavage fracture in a precracked bending specimen of HSLA steel is given in the following sub-sections:

2.1. Three Sequential Stages Comprising the Integrative Process of Cleavage Fracture

A typical process of cleavage fracture is composed of three sequential non-stop stages (schematically shown in Figure 1): the nucleation of a crack in a second phase particle at a dislocation pile-up (Figure 1 (a) and (b)); the propagation of the freshly nucleated second phase particle-sized crack into the matrix grain (Figure 1(c)); the propagation of the grain-sized crack into contiguous grains (Figure 1 (d)).

The crack nucleation in a second phase particle is caused by a dislocation pile-up driven by the effective shear stress at a critical plastic strain (Figure 1 (a) and (b)).

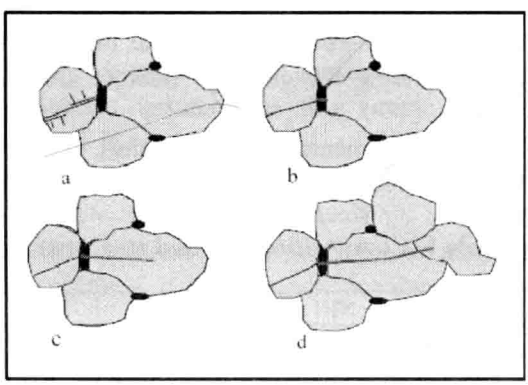

Figure 1. A schematics showing the three sequential steps comprising the cleavage fracture: (a) and (b) nucleation of a crack in a second phase particle at the end of a dislocation pile-up (c) propagation of the freshly nucleated second phase particle-sized crack into the matrix grain (d) propagation of the grain-sized crack into contiguous grains.